

WIENER FILTER ESTIMATION OF TRANSFER FUNCTIONS

ROBERT KESSEL

NAVAL RESEARCH LABORATORY

The use of a Wiener filter estimate for the linear transfer function can significantly improve the description of behavioral dynamics. This report presents a two-pass, Monte-Carlo-based algorithm that is well suited to repeated-trials local average measurements. The Wiener filter transfer functions strongly suppress noise artifacts as well as allow reliable transfer function determination under a much wider class of reinforcement schedules. Implications of expanding the possible form of experimental design are considered along with improvements in the fidelity of resulting predictions.

Key words: transfer function, Wiener filters, behavioral dynamics, linear systems analysis, Monte Carlo, pigeons

At an abstract level, before one moves to mathematical notation, any linear analysis of dynamics captures the system's invariant characteristics within a transfer function that relates inputs to outputs. In the specific case of steady-state behavioral dynamics, the transfer function relates an individual organism's time-dependent responding to the supporting, time-dependent, presentation of reinforcers. To the extent that an organism's behavior satisfies linearity, the same transfer function should hold equally well for any arrangement of reinforcers in time (i.e., reinforcement schedule) that an experimenter cares to employ. This invariance of the transfer function, irrespective of the supporting reinforcement schedule, sets the stage for a linear analysis to predict behavioral dynamics. Before such predictions can be tested, however, the technical challenge of computing a transfer function from data must be resolved.

Palya, Walter, Kessel, and Lucke (2002) found one method to estimate reliably a transfer function based on applying some specific restrictions to the baseline reinforcement schedule used to estimate the transfer function. Provided the restrictions are satisfied, the change in response rate over time

due to changing the schedule of reinforcement can be predicted. Palya et al.'s (2002) predictions have a reasonable level of fidelity, or agreement, to the observed behavior but are not flawless. In addition, even with a well-designed baseline reinforcement schedule, problems with noise exist. Both the restrictions upon the baseline reinforcement schedule and the noise problems can be alleviated by using the technique of Wiener filters.

To understand where Wiener filters fit within a linear analysis, it is necessary to restate both the defining expressions and the associated notation, and then to identify the transfer function within this framework. The linear analysis of McDowell, Bass, and Kessel (1993) relates an organism's behavior as a function of time, $B(t)$, to the prior history of reinforcement, $R(t')$, as a cumulative effect over the range of this history's possible times, t' with the expression

$$B(t) = \int R(t')G(t-t') dt'. \quad (1)$$

Equation 1 has a simpler form after conversion from time-dependent functions to frequency-dependent functions. The frequency domain form is completely equivalent from a mathematical standpoint. Applying a Fourier transform to both sides of Equation 1 yields

$$b(f) = r(f)g(f). \quad (2)$$

In Equation 2, lowercase functions denote frequency domain members of Fourier transform pairs. The corresponding time domain member of the pair is denoted with uppercase as in Equation 1. The factor $g(f)$ in Equation 2 is known as the transfer function

The author gratefully acknowledges the contributions of Bill Palya, Bob Lucke, and Greg Galbicka for helpful discussions on this algorithm and prior drafts of the paper, and Don Walter for extending his earlier data-reduction processing to yield the reinforcement and response variance blocks required by this research.

Address correspondence to Robert Kessel, Electro-Optics Technology Section, Code 8123, Naval Research Laboratory, Washington, D.C. 20375-5354 (e-mail: kessel@ncst.nrl.navy.mil). The software used in preparing this report is available from the JSU/SEBAC program archive at <http://www.jsu.edu/depart/psychology/sebac/wiener/>.

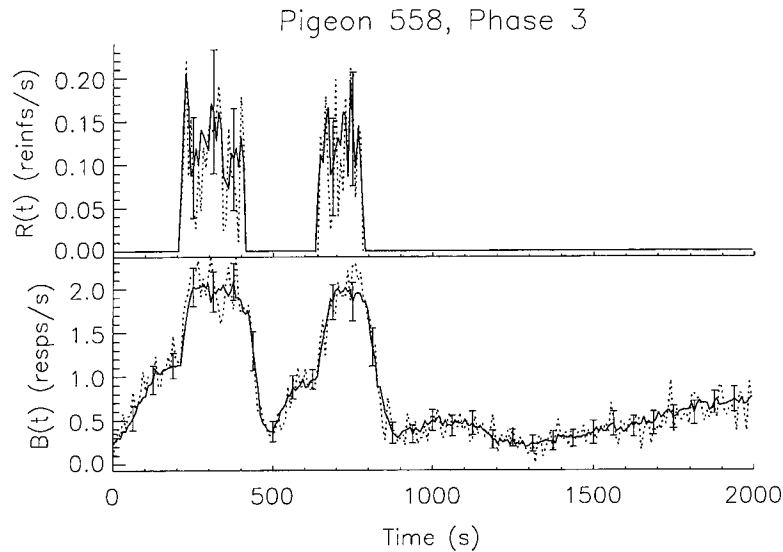


Fig. 1. The obtained reinforcement and response data across a trial for Pigeon 558 in Phase 3 from the data from Palya et al. (2002). The upper panel shows the obtained reinforcement rate in each time bin of the interval. The lower panel shows the obtained response rates. The SEM of every eighth time bin's reinforcement and response rates are shown by the superposed error brackets. The remaining error brackets, not shown for clarity, were the same local magnitude as those shown. The dotted curves shown in both plots are Monte Carlo copies generated from the obtained rate data.

and is, as noted above, a supposed characteristic of the organism itself. This report's central focus is a technique to compute $g(f)$ that is both numerically robust and applicable to a wider class of reinforcement schedules than the relatively restrictive forms used by Palya et al. (2002).

This report begins with a discussion of steps required for a linear analysis of steady-state behavior dynamics and the modifications necessary to include a Wiener filter. Next, the report covers the algorithm used to compute $g(f)$ from data. The report then discusses the results obtained by reanalyzing Palya et al.'s (2002) data. The report closes by briefly summarizing the implications and future applications of Wiener filter techniques.

EXTENDING LINEAR ANALYSIS WITH WIENER FILTER ESTIMATION

Palya et al.'s (1996, 2002) experimental studies of applying a linear analysis to behavioral dynamics have involved two (or more) experimental phases. In outline form, the basic design for a two-phase experiment is:

1. Use the obtained reinforcement rates $R_{b, \text{line}}(t)$ and obtained response rate

$B_{b, \text{line}}(t)$ from a first experimental condition (baseline phase) to estimate the transfer function $g(f)$.

2. Predict the response rate for a second experimental condition (test phase), $B_{\text{test}}^{\text{pred}}(t)$, from new reinforcement rates $R_{\text{test}}(t)$ and the previously estimated $g(f)$. The prediction is then compared to the obtained response rate $B_{\text{test}}(t)$.

All phases in Palya et al. used mixed schedules with brief intervals of a relatively rich reinforcement schedule, a variable-interval 20 s (VI 20 s), separated by longer intervals of extinction. As a colloquial shorthand, these brief unsignaled intervals inserted into a period of extinction during which the VI schedule operates are called *reinforcement pulses* or simply *pulses*. The analogous brief bursts of responding that are sometimes present in the observed behavior are also referred to as pulses. The solid curves in both panels of Figure 1 show the obtained reinforcement (top panel) and response rate (bottom panel) data from the initial baseline phase, in this case Phase 3, for Pigeon 558 (Palya et al., 2002).¹ The rates shown are repeated trials

¹ The data used in Figure 1 and for the balance of this

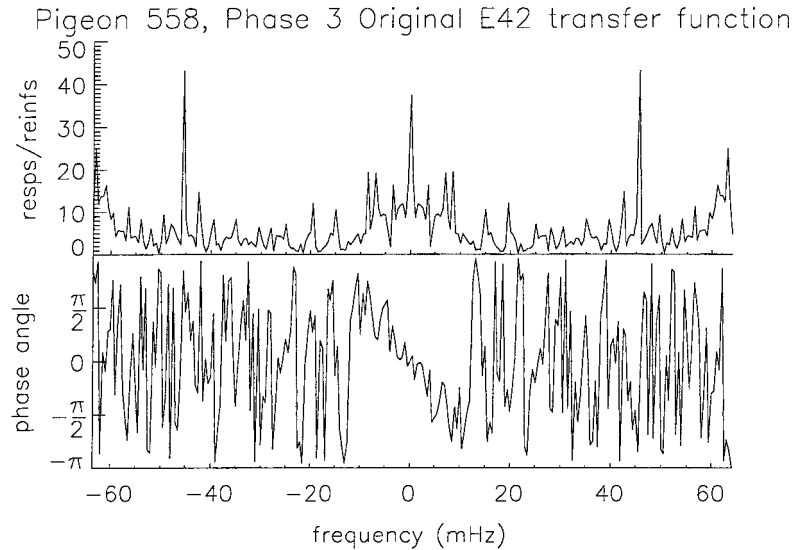


Fig. 2. The magnitude (upper panel) and phase, in radians (lower panel), for Pigeon 558's Phase 3 single-sample transfer function (b558_tfun.v1_p3.dat). The plot actually shows the complex conjugate of the original E42 result due to the sign change between IDL's definition of the Fourier transform and that of E42's *Numerical Recipes* based data reduction software.

local averages in which all data from the final 20 sessions of Phase 3 are combined in 256 contiguous bins across the common 2,000-s time scale and averaged. The use of a repeated trials experiment allows reinforcement and behavior, which appear in Equation 1, and local rates of reinforcement and behavior to be treated as equivalent measures. Also shown in Figure 1 are error brackets delineating the standard error of the mean (SEM). Note that during extinction, the reinforcement rate for all trials is exactly zero. Consequently, the SEM is identically zero and the error brackets merge into the mean. This zero-width distribution will have to be properly reflected when constructing the Monte Carlo copies of reinforcement data used below. The VI 20-s schedule results in a finite-width distribution of reinforcement rates during the two intervals of the reinforcement pulses. In contrast, the response distribution has a finite width throughout the trial. This summary of Palya et al.'s (1996, 2002) experiments is intended to illustrate the basic characteristics of the data and establish the nota-

report, as well as other results, are available at <http://www.jsu.edu/depart/psychology/sebac/linear-modeling/>. Note that this experiment's internal designation at JSU is E42, and it often is used as label and within data filenames.

tion used in the balance of this paper. (For a complete discussion of these experiments, see the original reports.)

The data reduction and analysis computer routines used by Palya et al. (2002) employed the simplest possible transfer function estimation method. One can obtain the expression

$$g_{E42}(f) = \frac{b_{b.\text{line}}(f)}{r_{b.\text{line}}(f)} \quad (3)$$

directly from Equation 2. The internal JSU designation "E42" subscript appears in Equation 3 to denote explicitly that experiment's data analysis method in contrast to the Wiener filter method developed below. From a purely analytic viewpoint, Equation 3 is the transfer function. However, as Palya et al. (2002) noted, use of a simple quotient for the transfer function gives rise to problems of numerical robustness and sensitivity to noise. As an example, Figure 2 shows the transfer function obtained by Palya et al. (2002) for Pigeon 558 during Phase 3. The sharp resonance spikes at ± 45 mHz in the upper panel are a processing artifact due to $r_{b.\text{line}}(f)$'s amplitude dropping close to zero near these frequencies. Behaviorally, such resonance spikes would correspond to strong 22-s period oscillation in the response rate, a finding

that is not seen in the data. More broadly, Palya et al.'s (2002) results and those of other workers studying behavioral dynamics on a fine scale (Higa, 1996; Higa & Pierson, 1998; Horner, Staddon & Lozano, 1997) indicate that sharp transitions in reinforcement are not reflected in changes in behavior that occur faster than the variations of a 30 mHz frequency. This implies that the transfer function corresponds to some form of low-pass filter with a cutoff frequency of about 30 mHz. Consequently, most of the narrow higher frequency spikes present in Figure 2 are probably traceable to division-by-near-zero errors in Equation 3.

To use a Wiener filter estimate for the transfer function, Equation 3 is replaced by

$$g_{\text{Wiener}}(f) = \frac{b_{\text{b.line}}(f)r_{\text{b.line}}(f)^*}{|r_{\text{b.line}}(f)|^2 + \left[\frac{\alpha}{\text{snr}(f)}\right]^2}, \quad (4)$$

where $r_{\text{b.line}}(f)^*$ is the complex conjugate of $r_{\text{b.line}}(f)$. It has been shown (Gonzalez & Wintz, 1987, pp. 229–232; Jain, 1989, pp. 276–282) that Equation 4 is the best estimator, in a least-squares sense, of a transfer function in the presence of uncorrelated measurement noise.

The second term in Equation 4's denominator is, in essence, a reciprocal signal-to-noise ratio (SNR). The specific signal-to-noise ratio used in Equation 4, $\text{snr}(f)$, is a frequency domain function (cf. Equation 2), and, like any SNR, it defines a relative precision, that is, a dimensionless ratio of a mean to a standard deviation. Because both $R_{\text{b.line}}(t)$ and $B_{\text{b.line}}(t)$ are subject to measurement noise, the SNR used in Equation 4 will include influences from both. The conversion of the time domain uncertainties of $R_{\text{b.line}}(t)$ and $B_{\text{b.line}}(t)$ to a frequency domain SNR is considered extensively in the next section. The numerator α is a tuning parameter that can be used in some circumstances, though not in the present case, to speed numerical convergence. In the absence of prior knowledge, $\alpha = 1$, and the second denominator term becomes exactly a reciprocal signal-to-noise ratio. The presence of a reciprocal signal-to-noise ratio plays an important role in Equation 4. For those frequencies where $b_{\text{b.line}}(f)/r_{\text{b.line}}(f)$ has a high SNR, Equation 4 closely approximates

Equation 3. For those frequencies where $r_{\text{b.line}}(f)$ is very close to zero, the SNR will be correspondingly low, and the reciprocal signal-to-noise ratio will suppress the troublesome spikes in $g(f)$.

Once $g_{\text{Wiener}}(f)$ is estimated with Equation 4, the second phase of the analysis outlined above proceeds without change. Equation 2 is used with the test phase reinforcement and $g_{\text{Wiener}}(f)$ to predict the frequency-domain representation of the responding as

$$b_{\text{test}}^{\text{pred}}(f) = r_{\text{test}}(f)g_{\text{Wiener}}(f). \quad (5)$$

The time-domain form of the predicted responding follows after application of an inverse Fourier transform:

$$B_{\text{test}}^{\text{pred}}(t) = \text{FT}^{-1}[b_{\text{test}}^{\text{pred}}(f)]. \quad (6)$$

Both $b_{\text{b.line}}(f)$ and $r_{\text{b.line}}(f)$ can be computed directly from data using a standard Fast Fourier Transform (FFT) routine. This leaves only the determination of $\text{snr}(f)$ before Equation 4 can be used.

TWO-PASS MONTE CARLO ALGORITHM FOR WIENER TRANSFER FUNCTIONS

The signal-to-noise ratio, $\text{snr}(f)$, appearing in Equation 4 is a measure of the precision with which the transfer function is known. Any SNR expresses this precision as a ratio of a mean (or signal) to a standard deviation (or noise). To foreshadow a bit, Equation 12 will be a ratio of exactly this form. Also, as already noted, $\text{snr}(f)$ is a function of frequency. Experimentally, $R_{\text{b.line}}(t)$ and $B_{\text{b.line}}(t)$ are measured as a function of time, as are their associated uncertainties that appear as the error bars in Figure 1. Consequently, the determination of $\text{snr}(f)$ requires a method to convert the relative precision of $R_{\text{b.line}}(t)$ and $B_{\text{b.line}}(t)$ into the corresponding information for an associated function of frequency. One method to make this conversion from the precision information for experimental, time-domain measures to the relative precision in the frequency domain needed for $\text{snr}(f)$ is based on a Monte Carlo. A Monte Carlo has the added merit of being convenient from the viewpoint of numerical software development.

For the present case, an appropriate Monte Carlo (MC) builds up N_{MC} copies of $R_{\text{b.line}}(t)$ and $B_{\text{b.line}}(t)$ using a set of ran-

dom numbers that match, in a statistical sense, the measured data itself. As a specific example, consider the 256 time bins of the i th Monte Carlo copy $R_{MC,i}(t)$. For each time bin, $1 \leq t_j \leq 256$, the Monte Carlo's value is the sum of $R_{b, \text{line}}(t_j)$ and a call to a Gaussian random number generator with its standard deviation equal to the uncertainty in that time bin, $\sigma_{R_{b, \text{line}}(t_j)}$. Because a Gaussian random number generator returns positive and negative values with a distribution that is symmetric and zero centered, the limit of the average of the Monte Carlo copies is the original data. Expressed as an equation, this limit is

$$\lim_{N_{MC} \rightarrow \infty} \frac{1}{N_{MC}} \sum_{i=1}^{N_{MC}} R_{MC,i}(t_j) = R_{b, \text{line}}(t_j), \quad (7)$$

for all j . The far stronger constraint of exact identity applies during the extinction intervals present in the schedule given by

$$R_{MC,i}(t_j) \equiv R_{b, \text{line}}(t_j), \quad (8)$$

for all i where t_j is in an extinction interval. The dotted curve in the top panel of Figure 1 shows an example $R_{MC,i}(t_j)$. Combining this i th Monte Carlo copy of $R_{b, \text{line}}(t_j)$ with remaining copies, yields the N_{MC} element set $\{R_{MC,1}(t_j), R_{MC,2}(t_j), \dots, R_{MC,i}(t_j), \dots, R_{MC,N_{MC}}(t_j)\}$. Using the same procedure and $256 \times N_{MC}$ additional calls to a Gaussian random number generator, one can generate the corresponding set of Monte Carlo copies of the measured behavior $\{B_{MC,1}(t_j), B_{MC,2}(t_j), \dots, B_{MC,i}(t_j), \dots, B_{MC,N_{MC}}(t_j)\}$. The bottom panel of Figure 1 shows an example $B_{MC,i}(t_j)$ with a dotted curve.

To get from these paired Monte Carlo copy sets to the Wiener filter transfer function requires two passes over the sets. During the first pass, one computes a transfer function for each of the N_{MC} Monte Carlo copy pairs using Equation 3 as

$$g_{MC,i}(f) = \frac{b_{MC,i}(f)}{r_{MC,i}(f)}. \quad (9)$$

The average of these N_{MC} transfer functions, given by

$$\begin{aligned} \overline{g_{MC}}(f) &\equiv \langle g_{MC,i}(f) \rangle \\ &= \frac{1}{N_{MC}} \sum_i^{N_{MC}} g_{MC,i}(f), \end{aligned} \quad (10)$$

will approach $g_{E42}(f)$ in the limit of sufficiently large N_{MC} . In the present case, I found that for $N_{MC} = 4096$, $\overline{g_{MC}}(f)$ would closely mimic $g_{E42}(f)$'s predictions for $B_{\text{test}}^{\text{pred}}(t)$. The averaging in Equation 10 does suppress the high frequency spike artifacts in $\overline{g_{MC}}(f)$ when compared to $g_{E42}(f)$. This spike artifact suppression in $\overline{g_{MC}}(f)$ occurs because, although each $g_{MC,i}(f)$ will have a spike artifact or two present, the specific frequency of the artifacts varies due to the random number construction of the Monte Carlo sets. Consequently, the isolated spikes that are due to a chance configuration driving $r_{MC,i}(f)$ close to zero will be washed out. However, those structures in $b_{MC,i}(f)$ and $r_{MC,i}(f)$ that are reliably generated in all Monte Carlo copies will add constructively when computing the average.

More important than gaining some suppression of the spike artifacts is using $\{g_1(f), g_2(f), \dots, g_i(f), \dots, g_{N_{MC}}(f)\}$ to determine $\text{snr}(f)$. This can be done by defining a standard deviation, as a function of frequency, with the expression

$$\begin{aligned} \sigma_{\overline{g_{MC}}}(f) &= \sqrt{\frac{1}{N_{MC} - 1} \sum_i^{N_{MC}} [g_i(f) - \overline{g_{MC}}(f)]^2}. \end{aligned} \quad (11)$$

A signal-to-noise ratio estimate can then be computed as

$$\text{snr}(f) = \frac{|\overline{g_{MC}}(f)|}{|\sigma_{\overline{g_{MC}}}(f)|}. \quad (12)$$

By construction, Equation 12's $\text{snr}(f)$ is common to all of the Monte Carlo pairs of $R_{MC,i}(t_j)$ and $B_{MC,i}(t_j)$. The absolute values appear in Equation 12 so $\text{snr}(f)$ will be a real-valued function rather than complex-valued as is the case for $\overline{g_{MC}}(f)$ and $\sigma_{\overline{g_{MC}}}(f)$. Figure 3 shows $\text{snr}(f)$ from Equation 12 for Pigeon 558's Phase 3 data. Note that whereas the lower frequency components are well determined, for frequency magnitudes greater than about ± 50 mHz the signal-to-noise ratio drops repeatedly below 1.0. For frequencies outside this limit, the transfer function is as dependent upon measurement noise as upon the underlying behavioral dynamics. Note that a precise determination of this noise floor limit is not required for the use of Equations

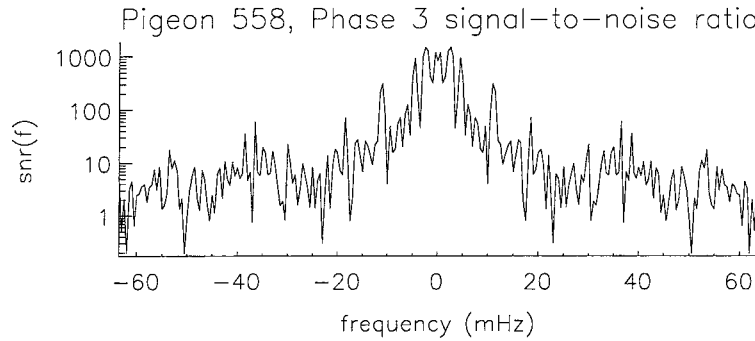


Fig. 3. The signal-to-noise ratio, $\text{snr}(f)$, of Pigeon 558's Phase 3 transfer function estimate.

tion 4. As a general guideline, though, one does want to select a sampling rate and the associated frequency scale so the $\text{snr}(f) = 1.0$ limit is reached near the maximum FFT frequency component magnitude.

One method to obtain the Wiener transfer function uses a second pass over the paired Monte Carlo copy sets $\{R_{MC,1}(t_j), R_{MC,2}(t_j), \dots, R_{MC,N_{MC}}(t_j)\}$ and $\{B_{MC,1}(t_j), B_{MC,2}(t_j), \dots, B_{MC,N_{MC}}(t_j)\}$. For each Monte Carlo pair, one can compute an individual transfer function using Equation 4 as

$$g_{w,i}(f) = \frac{b_{MC,i}(f)r_{MC,i}(f)^*}{|r_{MC,i}(f)|^2 + \left[\frac{1}{\text{snr}(f)}\right]^2}, \quad (13)$$

where $\alpha = 1$ and $\text{snr}(f)$ is the common estimate from Equation 12. The overall Wiener filter transfer function then follows immediately upon averaging as

$$\overline{g_w}(f) \equiv \langle g_{w,i}(f) \rangle = \frac{1}{N_{MC}} \sum_i^{N_{MC}} g_{w,i}(f). \quad (14)$$

Figure 4 shows $\overline{g_w}(f)$ based on Pigeon 558's Phase 3 data.

IMMEDIATE AND FURTHER USES OF WIENER TRANSFER FUNCTIONS

Figure 5 shows observed behavior (solid curve) along with three predicted behaviors for Pigeon 558 during Phase 4. The three

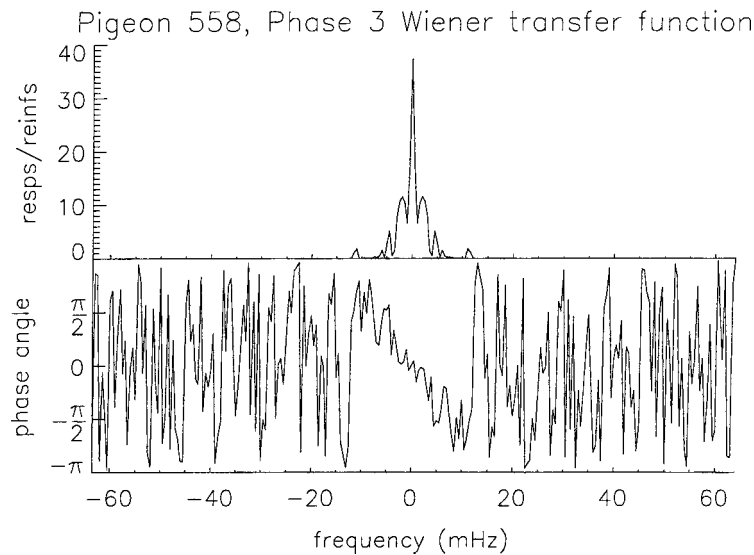


Fig. 4. The magnitude (upper panel) and phase, in radians (lower panel), for Pigeon 558's Phase 3 Wiener transfer function.

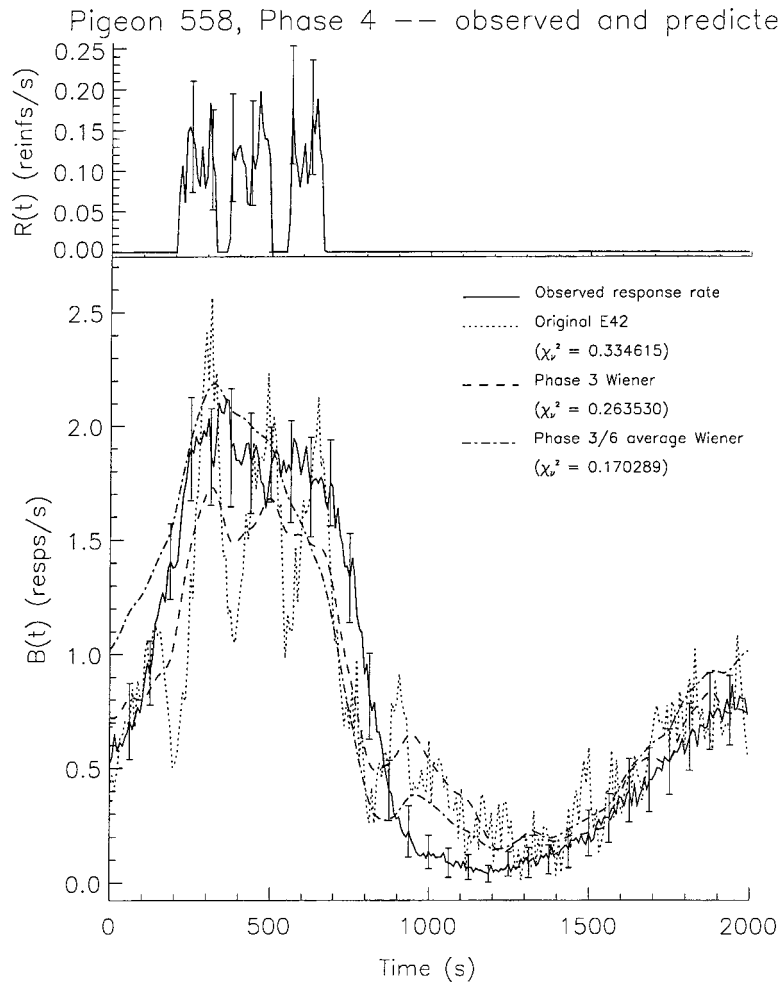


Fig. 5. The obtained reinforcement (upper panel) and response (lower panel) data across a trial for Pigeon 558 in Phase 4 from the data from Palya et al. (2002). Also shown are three different predictions for the response rates. The SEM of every eighth time bin's reinforcement and response rates are shown by the superposed error brackets. The remaining error brackets, not shown for clarity, were the same local magnitude as those shown.

predictions result from use of Equations 2 (or 5) and 6 with three different transfer functions. Note these are absolute predictions made without fitting parameters. The level of fidelity of each prediction is assessed quantitatively by reduced chi-square, χ_r^2 . For reference, a perfect prediction would agree with every observed response rate across the 2000-s trial and would have $\chi_r^2 = 0.0$. An immediate application of a Wiener filter transfer function is seen in the contrast between the prediction computed with the original $g_{E42}(f)$ (dotted curve) and $\overline{g_W}(f)$ (dashed curve). All the higher frequency oscillations present in the original prediction have been

suppressed along with excursions to impossible negative response rates. The Wiener filter transfer function prediction, for the most part, runs through the local average of the $g_{E42}(f)$ prediction. This is true for the other 4 pigeons and for all test phases of Palya et al.'s (2002) data. For this particular test reinforcement schedule with three relatively closely spaced VI 20-s pulses, the reduction in higher frequency oscillations improves the fidelity of the prediction to the observed behavior and χ_r^2 drops closer to zero. The reduction in χ_r^2 also was seen in the single pulse test phase. The Wiener filter predictions did not improve over those made with the origi-

nal simple estimate of Equation 3 for the test phase involving three relatively widely spaced VI 20-s pulses. As noted by Palya et al. (2002), widely spaced pulses will generate a strongly nonlinear ring or echo pulse of behavior. Consequently, improvements in the linear transfer function could not be expected to improve the prediction.

The use of Wiener filter transfer functions provides for more than the removal of the higher frequency spike artifacts. Because narrow frequency bands in which $r_{b, \text{line}}(f)$ has a near-zero amplitude do not generate a noisy transfer function, one is then free to extract transfer functions from a much wider set of baseline phases. For example, single pulse procedures will have strong division-by-near-zero problems in transfer function estimates at all multiples of the reciprocal pulse period (Palya et al., 1996). A Wiener filter transfer function based on a single pulse phase, in contrast, will be relatively free of these computational artifacts. Further, the Wiener filter's comparatively small transfer function in those frequency bands with low SNR simplifies averaging transfer functions obtained in different baseline phases. Low SNR bands are blocked, at the outset, from having an effect on the average with other transfer functions. This is greatly preferable to averaging transfer functions estimated directly from Equation 3, which give equal weight to all frequency regions.

The final prediction in Figure 5 illustrates combining the new capabilities to extract a reliable transfer function from a single pulse schedule and average transfer functions from different schedules. The prediction employs the average of a two-pulse Wiener transfer function (Phase 3) and a single-pulse Wiener transfer function (Phase 6) (dashed-dotted curve in Figure 5).

CONCLUSIONS

The Wiener filter transfer function algorithm resolves the difficulties that stem from

a division-by-near-zero condition occurring in Equation 3. This lifts restrictions in applying a linear analysis to behavioral dynamics in two ways. The Wiener algorithm provides an immediate sharp reduction in spike artifacts and sensitivity to measurement noise. It also opens up new classes of experimental study. The experimenter is freer in the design of baseline and test phases. This freedom can allow for experiments that employ unrestricted changes in the pulse locations, width, and even time-varying profiles in reinforcement rate. Such a wider class of experimental designs should make it possible to sort those aspects of behavioral dynamics that are well described by an assertion of linearity from those that are not. Determining the boundaries of nonlinearity can be an important first step towards understanding the processes that generate the nonlinearity.

REFERENCES

- Gonzalez, R. C., & Wintz, P. A. (1987). *Digital image processing* (2nd ed.) Reading, MA: Addison-Wesley Publishing.
- Higa, J. J. (1996). Dynamics of time discrimination: II. The effects of multiple impulses. *Journal of the Experimental Analysis of Behavior*, *66*, 117–143.
- Higa, J. J., & Pierson, D. (1998). Temporal control in rats: Analysis of nonlocalized effects from short interfood intervals. *Journal of the Experimental Analysis of Behavior*, *70*, 35–43.
- Horner, J. M., Staddon J. E. R., & Lozano, K. K. (1997). Integration of reinforcement effects over time. *Animal Learning & Behavior*, *25*, 84–98.
- Jain, A. K. (1989). *Fundamentals of digital image processing*. Englewood Cliffs, NJ: Prentice-Hall.
- McDowell, J. J., Bass, R., & Kessel, R. (1993). A new understanding of the foundation of linear system theory and an extension to nonlinear cases. *Psychological Review*, *100*, 407–419.
- Palya, W. L., Walter, D. E., Kessel, R., & Lucke, R. (1996). Investigating dynamic behavior with a fixed-time extinction schedule and linear analysis. *Journal of the Experimental Analysis of Behavior*, *66*, 391–409.
- Palya, W. L., Walter, D. E., Kessel, R., & Lucke, R. (2002). Linear modeling of steady-state behavioral dynamics. *Journal of the Experimental Analysis of Behavior*, *77*, 3–27.

Received December 10, 2003
Final acceptance May 7, 2004